Organic/Inorganic Hybrid Epoxy Nanocomposites from Aminophenylsilsesquioxanes

Jiwon Choi,‡ Seung Gyoo Kim,† and Richard M. Laine*,†,‡

Department of Materials Science and Engineering and the Macromolecular Science and Engineering Center, University of Michigan, Ann Arbor, Michigan 48109-2136

Received June 6, 2003

ABSTRACT: Selected epoxy-functionalized cube nanocomposites were prepared from octa(aminophenyl)-silsesquioxane (OAPS), poly(aminophenyl)silsesquioxane (PAPS), octa(dimethylsiloxypropylglycidyl ether) silsesquioxane (OG), diglycidyl ether of bisphenol A (DGEBA) and diaminodiphenylmethane (DDM). A systematic comparison of properties was conducted using GPC, FTIR, ^{29}Si NMR, TGA, and DMA. In these studies, we find that (1) tethers with aromatic components increase char yields and decomposition temperatures, (2) cube loadings are important in thermal stabilities, (3) aromatic tether structure, short lengths and high cross-link densities reduce tether segmental relaxation motions which in turn stiffen the network and minimize macroscopic glass transitions. Finally, nanocomposites prepared from OAPS and PAPS exhibit nearly identical thermomechanical properties with PAPS offering a low cost alternative to OAPS.

Introduction

In the search for advanced materials with novel properties, materials synthesis strategies have targeted reducing the dimensions of the constituent components in composites to the nanoscale to form nanocomposites.[1−8] One motivation for this approach lies in the knowledge that when component sizes approach those of molecules (a few nanometers), interfacial interactions will strongly influence global properties in ways that cannot be predicted by the simple rule of mixtures.[9−16] Equally important, incorporation of nanosized components also offers the potential to greatly improve the reproducibility of composite properties because complete control of the smallest building segments offers the best potential for controlling macroscopic properties. Finally, detailed structure-processing-property studies of nanocomposites should eventually permit properties prediction and application toward specific tailoring of properties.

In this regard, the nano building block approach offers a powerful tool to control structure at the nanoscale because not only the building segments but also their macroscopic organization can be controlled completely. That is, systematic construction of nanocomposites using selectively designed building blocks offers an excellent chance to develop and tailor novel properties. However, to assemble the right segments in forming building blocks and to process them properly for target properties, a thorough understanding of nanostructure-processing-property relationships in nanocomposites is critical.

To better understand these relationships in nanocomposites, we recently initiated a series of studies using well-defined silsesquioxane nanocomposites.[17,18] Our early research focused on developing a repertoire of functionalized octahedral silsesquioxane (cube) macromonomers as a starting point for formulating nanocomposites with the objective of determining whether well-defined monomer/composite nanostructures and periodically placed organic/inorganic components might offer novel and predictable properties. To date, we have successfully generated macromonomers based on cubes functionalized with methacrylate, epoxide, alcohol, and aliphatic amine groups and made nanocomposites from many of them.[17−24] Complementary work on epoxy-based silsesquioxane materials by Mather et al. and Pittman et al. has also been described recently.[26,27] Scheme 1 illustrates the formation of nanocomposites from functionalized cubic silsesquioxanes.

Our earlier nanocomposite work suggested that the structure and rigidity of the organic tethers connecting the cubes strongly mediate thermal stabilities, glass transition temperatures, and, consequently, global mechanical properties. These findings prompted us to search for routes to more rigid and thermally stable alternatives. In this regard, we recently reported the synthesis of octaaminophenylsilsesquioxane (**OAPS**) as the first example of a rigid and thermally stable nanoconstruction site.[28] The aniline groups of OAPS offer versatility both as reaction sites from which other nano building blocks can be added and as starting points for generating other functional groups, thereby providing access to diverse and novel nanocomposites.[28]

OAPS also provides an opportunity to conduct comparative structure-processing-property studies vis-à-vis our previous epoxy cube nanocomposite studies.[17,18] In particular, comparison of well-defined networks with linear tethers (as opposed to bifurcated tethers, see below) enables one to investigate isolated single tether segmental motions because cooperative motions of multiple tethers are limited by cubes with eight cross-link junctions and thus global behavior represents individual tether segmental motions. For example, comparison of epoxy nanocomposites made with diaminodiphenylmethane (**DDM**) and epoxy-functionalized cubes with those made from OAPS and the diglycidyl ether of bisphenol A offers one the chance to study the effects of cube functional groups and tether architec-

* Address correspondence to this author. talsdad@umich.edu.
† Department of Materials Science and Engineering, University of Michigan.
‡ Macromolecular Science and Engineering Center, University of Michigan.

10.1021/ma030309d CCC: $27.50
Published on Web 12/13/2003

Scheme 1. Nanocomposite Formation (II) from Cubic Silsesquioxane (I) via Cross-Linking of Functional Groups R

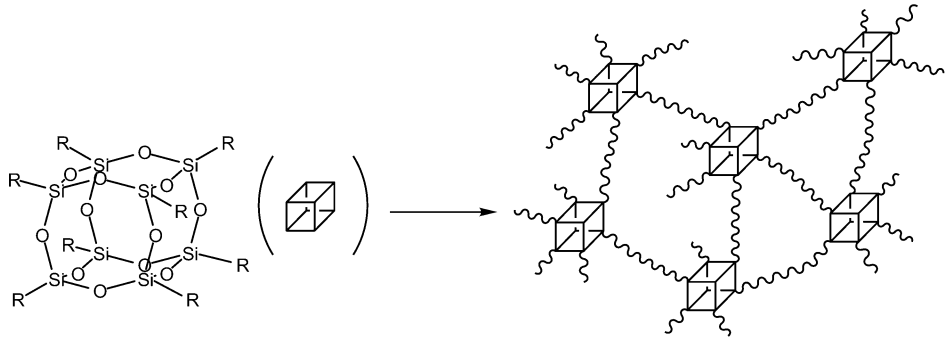

I II

Scheme 2. Epoxy Tether Formation Where One Component Is a Cubic Silsesquioxane

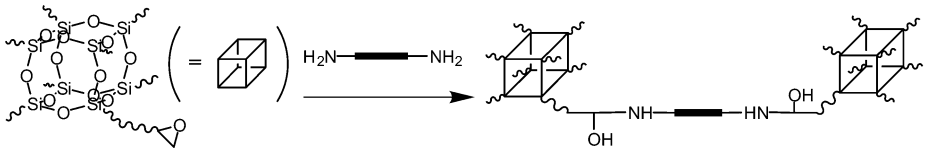

(a) Tether formation from epoxy cubes using DDM

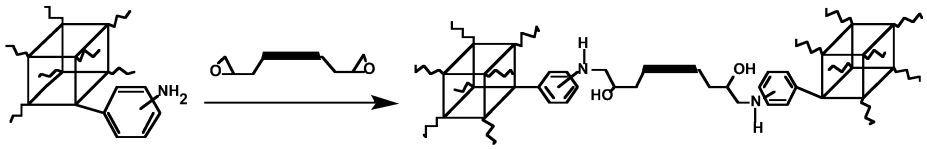

(b) Tether formation from OAPS and commercial epoxy, DGEBA.

Table 1. Formulation of Nanocomposites from OAPS, PAPS, DGEBAA, and OG

aminophenylcube/DGEBA nanocomposite	$N = 0.3$	$N = 0.5$	$N = 0.75$	$N = 1.0$
OAPS or PAPS	0.75 g (0.65 mmol)	1.11 g (0.96 mmol)	1.46 g (1.27 mmol)	1.74 g (1.51 mmol)
DGEBA	3.25 g (8.74 mmol)	2.89 g (7.77 mmol)	2.54 g (6.83 mmol)	2.26 g (6.08 mmol)
aminophenylcube/OG nanocomposite	$N = 0.3$	$N = 0.5$	$N = 0.75$	$N = 1.0$
OAPS or PAPS	0.61 g (0.53 mmol)	0.92 g (0.80 mmol)	1.24 g (1.07 mmol)	1.50 g (1.30 mmol)
OG	3.39 g (1.76 mmol)	3.08 g (1.60 mmol)	2.76 g (1.42 mmol)	2.50 g (1.30 mmol)

tures on tether segmental motions and thus macroscopic behavior as illustrated in Scheme 2. Similarly, nanocomposites prepared from both epoxy-functionalized cubes and OAPS allow one to examine how extremely high silica contents and short tether lengths affect composite properties.

Also of importance to our effort is making low-cost, equivalent rigid nano building blocks. In parallel to the development of functionalized octaphenyl cubes, we have applied identical reactions to polymeric phenyl silsesquioxanes (PPS) or phenyl "T" resins and successfully synthesized polyaminophenyl silsesquioxane (**PAPS**).[28] In our studies, no modification to the nitration and reduction reactions was necessary.[28] Therefore, comparison of OAPS and PAPS nanocomposite properties may justify the utility of PAPS as an alternative to OAPS.

We present here comparative studies of epoxy cube nanocomposites demonstrating that (1) nanocomposites prepared from OAPS and PAPS exhibit nearly identical thermomechanical properties, (2) tethers with more aromatic character provide better thermomechanical stabilities (as expected), and (3) nanocomposites with high silica contents and short tethers are quite thermally stable but quite brittle (as expected). To mirror previous studies, we used the diglycidyl ether of bisphenol A (**DGEBA**), a commercial epoxide and octaglycidyldimethylsiloxyoctasilsesquioxane (**OG**) as the epoxy cube.[17,18]

Experimental Section

Materials. The diglycidyl ether of bisphenol A (**DGEBA**) (DER 331, MW 372) was obtained from Dow Chemical Corp. (Midland, MI). Octaglycidyldimethylsiloxyoctasilsesquioxane [(glycidyl)$Me_2SiOSiO_{1.5})_8$] (**OG**)[18] (MW 1931.7) and octaaminophenylsilsesquioxane (**OAPS**)[25] (MW 1153.6) were synthesized following literature methods. Polyaminophenylsilsesquioxane (**PAPS**) was prepared from as-purchased polyphenylsilsesquioxane (PPS) (Gelest, PA) following the same method used for OAPS.

Processing. DGEBA/OAPS and DGEBA/PAPS Nanocomposites. In formulating DGEBA/OAPS composites, a variable N was defined as the molar ratio of NH_2 (in OAPS) to epoxy ring (in DGEBA). Thus, when $N = 1$, there are equal numbers of NH_2 and epoxy groups in the sample mixture. A conventional stoichiometric ratio of 2 mol of epoxy to 1 mol of amine would occur at $N = 0.5$.[29−32] An identical variable N was used for DGEBA/PAPS composites. Table 1 shows the formulations used for the various nanocomposites studied.

OAPS (PAPS) powder was weighed into a 20 mL glass vial containing a magnetic stir bar. THF (2 mL) was added to the vial and the OAPS (PAPS) dissolved completely on stirring. DGEBA was then added to the solution and the mixture was stirred to give a homogeneous solution. The dark yellow, transparent solution was then transferred to an aluminum mold (30 mm × 13 mm × 30 mm) preheated at 50 °C. THF was slowly removed under vacuum at this temperature. Following removal of solvent (30 min), the mixture was cured for 12 h at 50 °C, then 6 h at 100 °C, and finally 6 h at 150 °C under N_2. This process results in complete curing as we have reported elsewhere.[17] The rough edges of the cured sample were removed by polishing with SiC paper prior to DMA testing.

OG/OAPS and OG/PAPS Nanocomposites. The variable N (defined above) was used to formulate OG/OAPS and OG/PAPS specimens as shown in Table 1. OG/OAPS and OG/PAPS are processed following the same method as described above with modification of the cure conditions because of the poor miscibility of OAPS/PAPS with OG. THF solutions of OAPS (PAPS) with OG were heated at 40 °C for 10 h followed by slow removal of solvent under vacuum. The mixture was then cured for 24 h at 50 °C under N_2, followed by 6 h at 80 °C and then 6 h at 150 °C. Rough edges were removed as above. All samples were transparent under all cure conditions.

Characterization. Solid state ^{29}Si NMR spectra were obtained at 9 T using a Chemagnetics CMX-400 spectrometer operating at 79.5 MHz. Contact times were 2 ms and pulse delays were 20 s. The probe used was a Chemegnetics PENSIL design using 5 mm zirconia rotors at spinning rates of 3 kHz. The sample temperature was 30 °C and TMS was used as reference.

Fourier Transform Infrared Spectroscopy (FTIR). Diffuse reflectance IR spectra (DRIFTS) were obtained on macromonomer powders using a Mattson Galaxy Series FTIR 3000 spectrometer (Mattson Instruments, Inc.). Optical grade potassium bromide (KBr, International Crystal Laboratories, Garfield, NJ) was used as the supporting medium. Cured sample (5 mg) and KBr crystal (500 mg) were ground together using an alumina mortar and pestle. The ground powder was packed into a sample holder and leveled off with a glass plate to give a smooth surface. The holder was placed in the sample chamber and the spectrum was recorded under dry N_2 purge. At least 128 scans were averaged for each spectrum. The resolution was ±4 cm^{-1}.

Gel Permeation Chromatography (GPC). Molecular masses and distributions of OAPS and PAPS were measured using a Waters GPC system, equipped with RI and UV detectors, a Styragel column set (7.8 × 300, HR-high resolution 0.5, 1, 3, 4), and a PL-DCU data capture unit. These four columns are suitable for measuring small molecular masses with epoxy and amine functionalities. The system was calibrated using polystyrene standards. THF was used as the eluent, at a flow rate of 1.0 mL/min. GPC was also used to analyze the tether structures following dissolution of the core (see below).

Thermal Gravimetric Analysis (TGA). Thermal stabilities of materials under nitrogen or air were tested using a 2960 simultaneous DTA-TGA Instrument (TA Instruments, Inc., New Castle, DE). Samples (10−15 mg) were loaded in alumina pans, ramped to 1000 °C (5 °C/min/N_2) and mass change was recorded with reference to empty alumina pans. The N_2 or air flow rate was 60 mL/min.

Dynamic Mechanical Analysis (DMA). Dynamic mechanical behavior of cured samples was studied using a TA instruments 2980 dynamic mechanical analyzer (New Castle, DE). Cured samples were polished to ≈ 3.0 × 13.0 × 30.0 mm and mounted on a single cantilever clamp. The mechanical properties were measured under nitrogen in step mode every 10 °C from −50 to +200 °C. Prior to each measurement, the environment was kept at the setting temperature for 10 min to ensure thermal equilibration.

Cross-Link Density Calculations. Three different approaches were taken to calculate the number density of cross-linked chains, ν (mol/cm^3) and the average molecular weights of chains between cross-links, M_c.

(1) For DGEBA/DDM that follows the rubber elasticity theory,[31−34] ν and M_c were calculated as follows:

$$\nu = \frac{E}{3RT}, \quad M_c = \frac{\rho}{\nu}$$

where E is a rubbery state modulus (MPa), R is a gas constant (8.314 cm^{-3} KPa/mol·K), T is $T_g + 40$ °C (K) where the rubbery modulus is taken, and ρ is the density of DGEBA/DDM (assumed 1 g/cm^3).

(2) Because rubber elasticity theory does not work for the cube nanocomposites (see Discussion), ν and M_c of cube nanocomposites were calculated as follows. For fully cross-linked cube nanocomposites at $N = 1$ with "linear" tethers including DGEBA/OAPS (PAPS) (see Scheme 7), M_c is equal to the tether molecular weights. For example, for DGEBA/OAPS (PAPS), it is calculated as the sum of molecular weights of DGEBA (371) and two aniline groups (92) to give 555. The number density of cross-linked chains, ν is also equal to the number of tethers. Because one cube generates eight tethers, but one tether is shared by two cubes, ν can be estimated as follows:

$$\nu = (\text{moles of cubes in unit mass} \times 8)/2 \times \rho$$

where ρ is the density of cube nanocomposites (assumed as 1 g/cm^3). For DGEBA/OAPS (PAPS), it is estimated as 2.1×10^{-3} mol/cm^3.

(3) For cube nanocomposites consisting of "bifurcated" tethers including OG/DDM at $N = 0.5$ (see Scheme 7), one cube generates eight tether segments, but one full tether is shared by four cubes (two linear tethers meet to form one bifurcated tether). Also in one bifurcated tether, two cross-links connect five small segments. Thus, ν is estimated as follows:

$$\nu = \{5 \times (\text{moles of cubes in unit mass} \times 8)/4\} \times \rho$$

In this case, M_c is equal to one-fifth of the bifurcated tether molecular weight. For example, for OG/DDM at $N = 0.5$, ν is estimated as 3.7×10^{-3} mol/cm^3 and M_c is 191.

The number density of cross-link junctions, μ (mol/cm^3), was also calculated in a manner parallel to ν and M_c to better understand the networks of various shapes in study. For DGEBA/DDM at $N = 0.5$, μ was calculated as twice the moles of DDM in unit volumes (one DDM generates two cross-link junctions) and estimated to be approximately 2.1×10^{-3} mol/cm^3.

For cube nanocomposites with linear tethers, the number density is eight times the moles of cubes in unit volumes because one cube provides eight cross-links. For example, the value is estimated as 3.0×10^{-3} mol/cm^3 for DGEBA/OAPS.

For cube nanocomposites with bifurcated tethers, four bifurcated tethers having two cross-link junctions form per cube with one tether shared by two cubes. Thus, with four additional cross-link junctions per cube, μ is 12 times the moles of cubes. For example, it is estimated as 4.4×10^{-3} mol/cm^3 for OG/DDM at $N = 0.5$.

Results and Discussion

We describe here three comparative studies. The first concerns structure−property relationships in epoxy cube nanocomposites prepared using two different aminophenyl cubes. The second compares nanocomposites prepared from epoxy and amine functionalized cubes, respectively. Last, the effects of tether length, number density and silica content (as cube cores) on thermomechanical properties are examined using nanocomposites prepared from both amino- and epoxy-functionalized cubes.

In the following sections, we first characterize two macromonomers, octa(aminophenylsilsesquioxane) (**OAPS**) and poly(aminophenylsilsesquioxane) (**PAPS**)

Table 2. GPC (THF/polystyrene), TGA (N_2/5 °C/min), and FTIR[39] Data for OAPS/PAPS

		OAPS (MW 1153.7)	PAPS
GPC	M_n	1057	1410
	M_w	1133	1890
	M_w/M_n	1.07	1.34
TGA	T_d(5%)[a]	330	136
	T_d(20%)[b]	489	472
	CY[c]	41.1	41.4
FTIR (cm^{-1})		3370 (ν_{N-H}, w[d]), 3150−2820 (ν_{C-H}, m), 1600 ($\nu_{C=C}$, s), 1230−960 ($\nu_{Si-O-Si}$, s)	3360 (ν_{N-H}, w[d]), 3120−2830 (ν_{C-H}, m), 1100 ($\nu_{C=C}$, s), 1230−960 ($\nu_{Si-O-Si}$, s)

[a] T_d(5): 5% mass loss temperature under N_2 (°C). [b] T_d(20): 20% mass loss temperature under N_2 (°C). [c] CY: ceramic yield at 1000 °C under air (%). [d] w = weak, m = medium, s = strong.

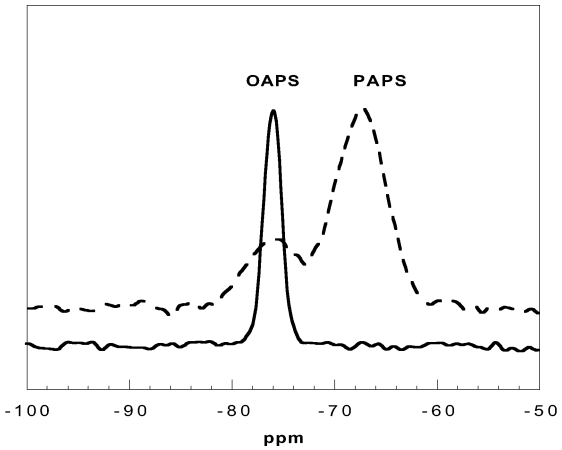

Figure 1. ^{29}Si MAS NMR of OAPS and PAPS.

by GPC, solid-state ^{29}Si SMR, and FTIR analyses followed by a discussion of materials selection criteria for comparative study. Then the diglycidyl ether of bisphenol A (**DGEBA**)/OAPS and DGEBA/PAPS nanocomposites are compared using DMA and TGA. The next section compares DGEBA/OAPS properties with those of previously studied octaglycidyldimethylsiloxyoctasilsesquioxane (**OG**)/diaminodiphenylmethane (**DDM**) nanocomposites[21] using TGA and DMA. Last, nanocomposites prepared using OG/OAPS and OG/PAPS mixtures are characterized by TGA and DMA.

Materials. OAPS vs PAPS. In our study, OAPS and PAPS were prepared via identical nitration/reduction reactions of octaphenylsilsesquioxane (OPS) and polyphenylsilsesquioxane (PPS). The major differences between OAPS and PAPS reside in the molecular weights and end groups. Selected analytical results are summarized in Table 2 and Figure 1, respectively.

These results suggest that PAPS consists primarily of partially condensed dimers and trimers ($M_n \sim 2300$) with some SiOH end groups (Scheme 3). In separate studies, we prepared high molecular weight PPS ($M_n \approx$ 17 000) however, the resulting PAPS products are essentially the same as starting from oligomeric PPS purchased from Gelest.[26,27] A partially condensed dimer structure has been reported in the literature[35] and is thought to closely resemble the structure of the PAPS oligomers. Note that the PAPS molecular weight in Table 2 is not quite twice that of OAPS because the

Scheme 3. Structure of OAPS (60:30:10 m:p:o) and Possible Structure for PAPS

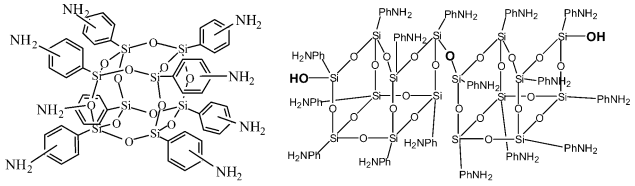

Scheme 4. Octaglycidyldimethylsiloxyoctasilsesquioxane (OG), Diaminodiphenylmethane (DDM), and Diglycidyl Ether of Bisphenol A (DGEBA)

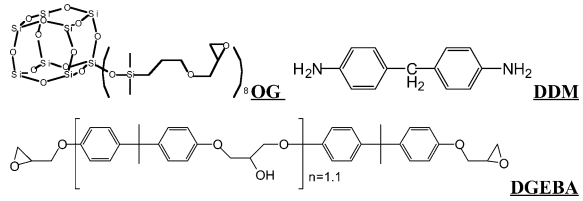

nonlinear changes in cube hydrodynamic volume leads to molecular weights that are not directly related to the polystyrene standards.

Although the νO−H band at 3300−3500 cm^{-1} in the FTIR spectra is hardly distinguishable from the νN−H peak at ~3300 cm^{-1}, ^{29}Si NMR spectra clearly show Si peaks at −68.0 and −76.0 ppm that represent T_2(Ph)(OR) and T_3(Ph), respectively.[36−38] In particular, T_2(Ph)(OR) is thought to contain only hydroxy groups (R = H) because potential alkoxy groups in the polyphenylsilsesquioxane starting materials are most likely removed during nitration (fuming nitric acid). The PAPS 5% mass loss temperature (~140 °C) is likely due to condensation reactions between these hydroxyls. The PAPS ceramic yield would be expected to be lower than that of OAPS because of the presence of uncondensed Si−OH units. However, the ceramic yield (41.4%) is higher than expected suggesting some Si units have lost phenyl groups forming Si−OH groups.

OG, DGEBA, and DDM. In earlier studies,[17,18] OG was chosen to reflect the glycidyl ether segment of DGEBA such that similar epoxy chemistries would result when OG and DGEBA were reacted with the same curing agent, DDM (Scheme 4). A similar approach was used for comparative studies replacing DDM with OAPS or PAPS. All three aromatic amines are structurally similar. The degree of condensation of DGEBA used throughout our studies is 1.1, and thus the "tethers" connecting cube vertices consisting of DGEBA/aniline groups can be considered to be well-defined.

The above nano building blocks provide the opportunity to extend our previous comparative structure−property studies to DGEBA/OAPS (PAPS) and OG/DDM nanocomposites. Scheme 5 shows the expected tether structures in these nanocomposites. Each tether forms from the reaction of two aniline moieties with two glycidyl epoxy groups creating very similar structures and lengths. The notable differences are that the DGEBA/OAPS tether has two more aromatic rings while the OG/DDM tether has two Si−O segments. Therefore, comparative studies should provide an understanding of the effects of higher aromatic contents on tether and global properties.

However, some conditions must be met before such comparisons can be considered legitimate. First, well-

Scheme 5. Comparison of Linear Tether Structures for DGEBA/OAPS and OG/DDM Nanocomposites[a]

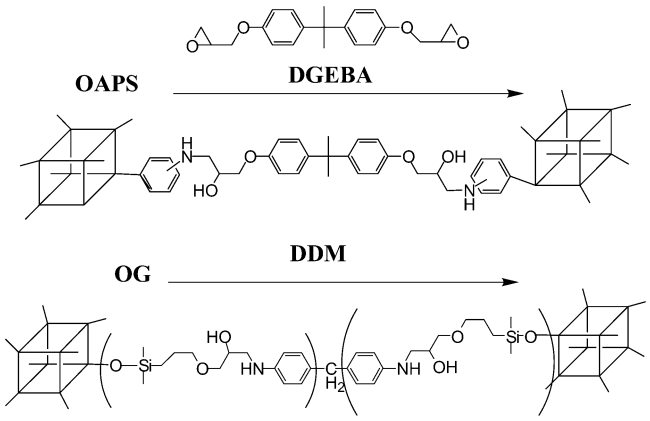

[a] DGEBA is shown as a monomer. The OG/DDM tether consists of two segments identical to OG/OAPS tethers (Scheme 7).

defined network architectures common to all composites must be developed such that the nanocomposites differ only in tether structure. In this light, networks consisting solely of linear tethers (Scheme 6, structure **I**) are most suitable because linearity is easily accessed by controlling the steric hindrance in the cure reaction[17,40] or by suppressing formation of bifurcated tethers (Scheme 6, structure **II**) through control of the reaction stoichiometry.[18] Next, cube nanocomposites must have minimal defects and similar cross-link densities such that only differences in the tether structure induce different network stabilities as addressed more extensively below.

The effects of cubes as inorganic cross-linkers can be studied by comparing DGEBA/OAPS with DGEBA/DDM. Here the networks consist of identical DGEBA/aniline segments and structural differences are caused only by introducing fully dispersed rigid silica particles as cube cores. In contrast, OG/OAPS (PAPS) nanocomposites offer the chance to study the effects of tether lengths on nanocomposite behavior because the OG/OAPS (PAPS) tether lengths are essentially half those of DGEBA/OAPS or OG/DDM tethers. Scheme 7 illustrates tether formation in these nanocomposites.

In the following sections, the thermomechanical properties of the above-described nanocomposite sets are compared using DMA and TGA. Selected DMA, TGA properties, tether shapes and cross-link densities of DGEBA/DDM, OG/DDM, and OC/DDM related to OG/DDM are shown in Table 3 for comparison and discussed thereafter. Table 3 also lists the properties of DGEBA/OAPS and OG/OAPS for comparison.

Some salient features of Table 3 data are discussed below. One assumption in this discussion is that the maximum cross-link densities of nanocomposites are identified by the highest glass transition temperatures as in epoxy thermosets (this argument was well justified in our previous publications[17−18,41]). However, for some nanocomposites, the existence of T_gs is unclear in the DMA measurements because of the unusually small decreases in the elastic moduli. In these cases, the maximum cross-link densities are assigned to the compositions where the decreases in elastic moduli are at a minimum over the examined temperature range (∼250 °C), and are listed as "no T_g" in the table.

Given this consideration, the stoichiometry for the maximum cross-link densities (highlighted in italic bold letters in the table) are found to vary depending on the nanocomposites. They are $N = 0.5$ for DGEBA/DDM and OG/DDM, and $N = 1$ for other systems. This is because the bifurcated tethers are maximized at $N = 0.5$ with minimum defects for the DGEBA/DDM and OG/DDM, while they do not form in other systems for any composition probably due to steric hindrance. Consequently, the OC/DDM system is highly defective at $N = 0.5$ whereas the $N = 1$ stoichiometry gives the highest number of cross-links. Model studies and direct tether shape assessment via ^{1}H NMR[18,41] in previous OG/DDM and OC/DDM studies suport this argument.

Note that for $N = 1$, the DGEBA/DDM system is expected to be primarily a linear polymer. Given that we previously found that even at $N = 1$ for the OG/DDM system, some fraction of bifurcated tethers do form for statistical reasons. We also assume that for the DGEBA/DDM $N = 1$ system, some bifurcations do occur; thus, it is anticipated that a low gel fraction will form within this material. Therefore, one might anticipate that above T_g, one would observe viscous flow; however, no effort was made to detect such behavior.

Of particular relevance are the different cross-link densities, M_c, ν, and μ as discussed in-depth in the DMA section below.

OAPS vs PAPS. Both OAPS and PAPS react readily with DGEBA. To enhance mixing, a minimum amount of solvent, e.g., acetone or THF (typically), was used to form homogeneous solutions. On vacuum evaporation of solvent, curing followed the same protocol (50 °C/12 h,100 °C/6 h,150 °C/6 h/N_2). The same formulation variable N as above was used for the DGEBA/OAPS and DGEBA/PAPS nanocomposites for ease of comparison. Scheme 5 shows the representative tether structure for DGEBA/OAPS.

Thermal Gravimetric Analyses (TGA). The thermal stabilities of DGEBA/OAPS and DGEBA/PAPS were examined using TGA (5 °C/mn/N_2) as given in Table 4. Both nanocomposites exhibit nearly identical thermal stabilities. Mass loss temperatures (5%) for DGEBA/PAPS are only slightly lower than for DGEBA/OAPS and the primary decomposition temperatures as measured by 20% mass loss are also similar at ∼390 °C. Char (N_2) and ceramic (air) yields are almost identical for both nanocomposites despite the partially condensed structures in PAPS.

In comparison, both nanocomposites produce significantly higher char yields (N_2) than the theoretical ceramic yields. Because measured ceramic yields (air) confirm the silica contents in the nanocomposites, these results indicate that the aromatic structures are responsible for excess char yields. This trend is also common for organic polymers.[42−48] Note that the 5% mass loss temperature for PAPS macromonomer is significantly lower than that of OAPS, despite the similar ceramic yields (Table 2), and likely reflects the presence of SiOH groups. These results suggest that structural defects in PAPS are not particularly significant. Furthermore, the initial mass loss ∼140 °C becomes insignificant when the relative fraction of hydroxyl groups is diluted on curing with DGEBA. One possible advantage to the presence of SiOH groups may be in the formation of bonds to surfaces suggesting utility for coatings applications.

Dynamic Mechanical Analysis (DMA). In cube nanocomposites, well-defined single segment tethers and cubes form networks. Because cubes are common to all nanocomposites, tether properties must be the

Scheme 6. Linear (I) and Bifurcated[18] (II) Tethers[a]

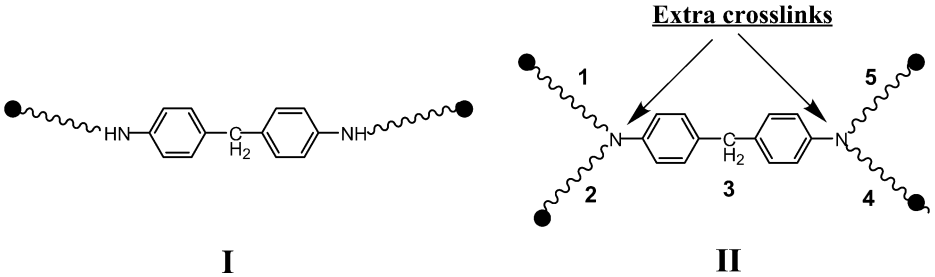

[a] Five segments connected via two cross-link junctions form bifurcated tethers connecting four vertexes (●). Linear tethers join two vertexes.

Scheme 7. Tether Formation in OG/OAPS and OG/PAPS[a]

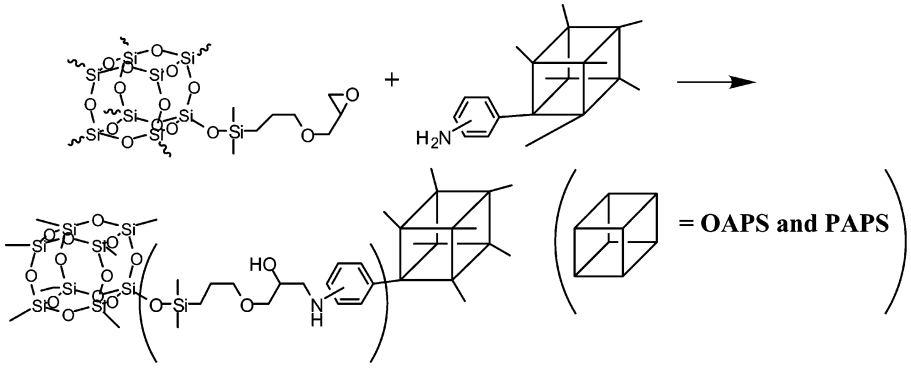

[a] Tether length (MW = 277 g/mol) is half that of DGEBA/OAPS (MW = 555 g/mol) or OG/DDM (MW = 577 g/mol) (Scheme 5).

Table 3. Selected DMA, TGA Properties, Tether Shapes, and Cross-Link Densities of DGEBA/DDM, OG/DDM, and OC/DDM Nanocomposites,[17,18,40,41] Where DGEBA/OAPS and OG/OAPS Properties Are Also Shown for Comparison.

composites	DGEBA/DDM	OG/DDM	[a]OC/DDM	DGEBA/OAPS	OG/OAPS
N at max. x link density (XD)	0.5	0.5	1.0	1.0	1.0
T_g at $N = 0.5$ (°C)[b]	160	no T_g	70	170	NA
T_g at $N = 1$ (°C)[b]	110	60	170	no T_g	NA
$N = 0.5$ rubbery modulus, MPa	25	NA	100	300	NA
$N = 1$ rubbery modulus, MPa	8	60	30	NA	NA
T_d(5%) at $N = 1$ (°C)[c]	338	344	415	355	385
T_d(20%) at $N = 1$ (°C)[d]	368	405	450	384	448
CY (%) at $N = 1$ (measured)[e]	0	32.0	31.0	17.6	46.2
CY (%) at $N = 1$ (theory)[f]	0	35.2	32.0	18.1	46.9
char yield (%) at $N = 1$ (N_2)	17	39.8	33.8	43	61
$N = 0.5$[g] primary tether shape	***bifurcated***	***bifurcated***	only linear	only linear	only linear
$N = 1$ primary tether shape	mostly linear	mostly linear	***only linear***	***only linear***	***only linear***
M_c (MW between cross-links)[h] at max. XD	474	191[i] (577)[i]	597	555	277
ν (no. of cross-linked chains)[h] at max. XD (mol/cm^3)	2.11×10^{-3}	3.68×10^{-3} [i] (1.47×10^{-3})[j]	1.43×10^{-3}	1.51×10^{-3}	2.60×10^{-3}
μ (no. of cross-link junctions) (mol/cm^3)	2.12×10^{-3}	4.42×10^{-3} [j] (2.94×10^{-3})	2.85×10^{-3}	3.02×10^{-3}	5.20×10^{-3}

[a] OC: octa(dimethylsiloxyethylcyclohexylepoxide)silsesquioxane. [b] T_g: determined by DMA. [c] T_d(5): 5% mass loss temperature under N_2 (°C). [d] T_d(20): 20% mass loss temperature under N_2 (°C). [e] CY(measured): ceramic yield at 1000 °C under air (%). [f] CY(theory): theoretical ceramic yield based on silica content. [g] Tether shape: determined by model curing study/direct tether investigation using GPC. [h] M_c, ν: values for OG/DDM and OC/DDM at $N = 1$ are calculated based on linear tether formation. See Experimental Section for details. [i] OG/DDM: tether MW = MW of one DDM + MW of four OG arms = 198 + 4 × 189.5 = 956; thus, effective $M_c' =$ tether MW/5, effective $\nu' = (\nu \times 5)/2$. [j] OG/DDM: values at $N = 1$ are shown for comparison. Linear tether formation is assumed.

variables that directly affect the macroscopic properties (given similar network architectures). Cubes are immobilized by eight cross-links on vertices and thus behave as anchors for tethers, limiting cooperative motions of multiple tethers. Thus, macroscopic glass transitions result primarily from a combination of individual tether relaxation motions. In other words, the macroscopic properties observed provide information about single tether properties. For example, glass transitions characterized by DMA probably represent isolated single tether relaxation motions.

However, cross-link density must also be considered in understanding the glass transition behavior associated with tether relaxation. For organic epoxy resins, rubber elasticity theory[31−34] is typically used to estimate cross-link densities in terms of molecular weights between cross-links (M_c) and the number of cross-linked chains (ν). However, this theory does not seem applicable for evaluating cube nanocomposites because they often do not exhibit rubbery behavior or T_g. Furthermore, the network structures can differ from those of organic rubbers because cubes offer extensive localized cross-linking. In this light, the cross-link densities of cube nanocomposites are better represented by the number of cross-links junctions because they can reflect the effects of cubes, which can provide up to eight

Table 4. TGA of Nanocomposites (N_2/5 °C/min) Prepared from OAPS/PAPS and DGEBA

	DGEBA/OAPS					DGEBA/PAPS			
N	T_d(5%) (°C)[a]	T_d(20%) (°C)[b]	char yield (%)[c]	CY (%)[d]	CY(theory) (%)[e]	T_d(5%) (°C)[a]	T_d(20%) (°C)[b]	char yield (%)[c]	CY (%)[d]
0.30	292	388	28	7.2	8.0	274	379	26	7.0
0.50	369	392	36	10.9	11.6	355	390	34	10.6
0.75	348	387	40	14.7	15.2	353	389	40	14.3
1.00	355	384	43	17.6	18.1	347	391	43	17.1

[a] T_d(5): 5% mass loss temperature under N_2 (°C). [b] T_d(20): 20% mass loss temperature under N_2 (°C). [c] Char yield at 1000 °C under N_2 (%). [d] CY: ceramic yield at 1000 °C under air (%). [e] CY(theory): theoretical ceramic yield based on silica contents.

junctions per cube. These points are further addressed as follows.

Network structural features of various nanocomposites are best discussed in terms of M_c, ν, and μ (see Experimental Section for calculation details). In this discussion, T_gs are compared at maximum cross-link densities unless stated otherwise.

M_c is defined as the molecular weight between cross-links and represents the average size of the basic "tether building blocks" for linear tethers. Thus, with small M_c, networks are expected to be stiffer than the ones with higher M_c to give higher T_gs. For organic epoxy thermosets,[31−34] this is usually true. However, this general rule does not hold between organic thermosets and cube nanocomposites. For example, M_c of DGEBA/DDM (474) is smaller than that for OC/DDM (597) or DGEBA/OAPS (555) yet gives the lowest T_g. In our studies of cube nanocomposites, these "high or No T_gs" were observed for an M_c range of 200−600. These features are because the "binding", or cross-linking of tether building blocks in cube nanocomposites are highly localized on cubes to produce globally rigid networks even with longer linear building blocks. Similar patterns are found in ν, No. of cross-linked chains. ν represents the spacial density of linear building blocks. ν's of OC/DDM and DGEBA/OAPS are lower than that of DGEBA/DDM, yet they show higher T_gs.

The rubber elasticity theory, if applied to cube nanocomposites, results in huge disprepancies in M_c and ν from our estimation. For example, for DGEBA/OAPS, rubber elasticity theory gives M_c and ν as 43 and 23 mmol/cm^3, respectively (with $E = 0.3$ GPa and $T = 550$ K), vs 555 and 1.5 mmol/cm^3 reported in Table 3.

However, when μ, number of cross-link junctions is considered, these observations can be explained. The μ of nanocomposites (>2.8 mmol/cm^3) is always higher than for DGEBA/DDM (∼2.1 cm^3). Here μ can be up to twice as high as that of DGEBA/DDM where no T_g is observed. These different anticipations by the rubber elasticity theory and the consideration of μ originate from the fact that the rubber elasticity theory fails to grasp the role of cubes in networks. That is, cube nanocomposites are unique in terms of network structures and must be separated from the conventional theory in anticipating properties. In this particular case of cross-link densities, μ is more appropriate in narrowing the gap between organic and cube thermosets.

The DMA results for DGEBA/OAPS and DGEBA/PAPS are presented in Figures 2 and 3. These profiles (Figure 2) exhibit three distinct but similar features with the DGEBA/OAPS moduli being consistently but only slighly higher. The DGEBA/OAPS profiles are almost identical for $N = 0.75$ and 1.00 exhibiting no T_gs, while T_g diappears completely only at $N = 1.0$ in DGEBA/PAPS. This slightly delayed disappearance of T_g may arise because the partially condensed PAPS

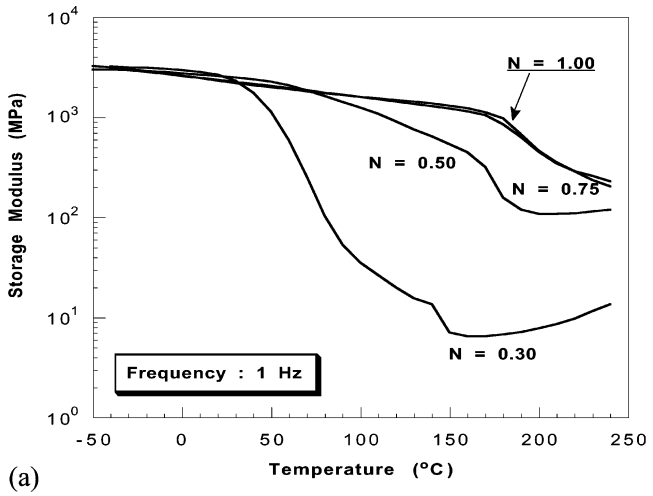

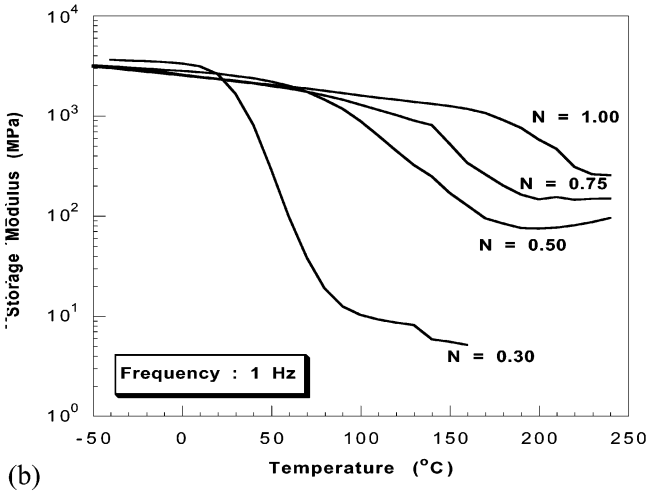

Figure 2. DMA storage moduli for nanocomposites: (a) OAPS/DGEBA; (b) PAPS/DGEBA. Both of them were cured following the same cure protocol (50 °C,12 h/10 °C, 6 h/150 °C, 6 h/N_2).

structures are somewhat less rigid than OAPS, resulting in a less rigid network and lower T_gs at equivalent Ns. However, this discrepancy becomes insignificant at $N \approx 1$, where networks have maximum cross-link densities (3.0×10^{-3} mol/cm^{-3} vs $\approx 2 \times 10^{-3}$ mol/cm^{-3} for organic epoxy) and rigid tethers, minimizing the softening effect of PAPS.

The highest rubbery modulus is observed at $N \approx 1$, suggesting that the highest cross-link density is obtained when equal amounts of NH_2 and epoxide react to form linear tethers. In previous epoxy nanocomposites studies (Table 3), this was the case when bulky cyclohexyl epoxides[17,40] limited the reaction of epoxide groups

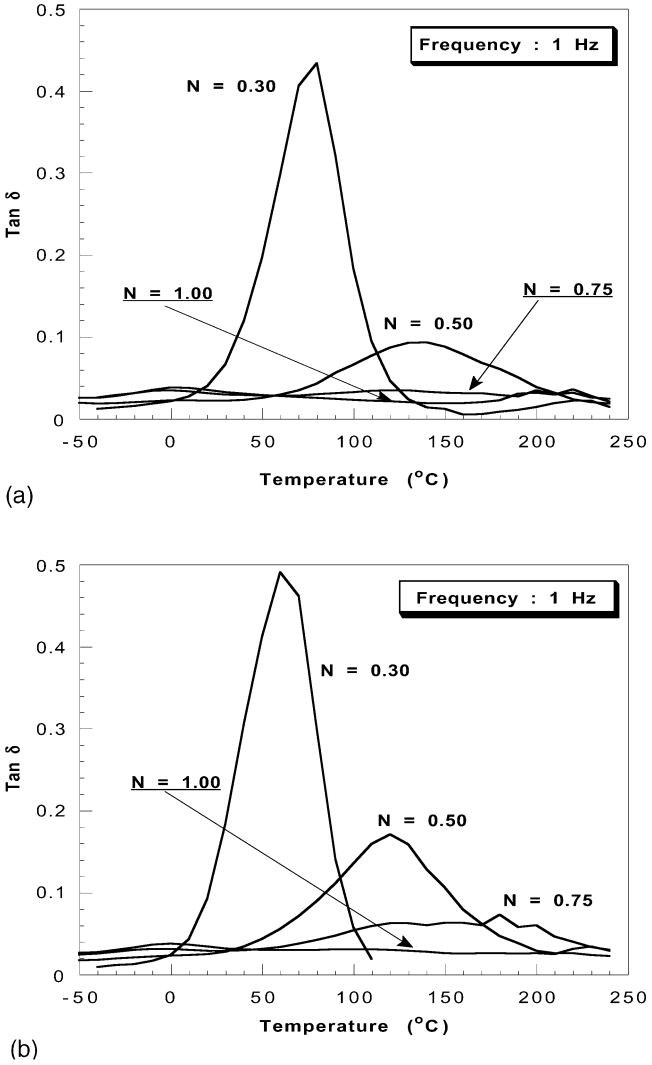

Figure 3. DMA tan δ for nanocomposites: (a) OAPS/DGEBA; (b) PAPS/DGEBA.

with secondary amines, leading to linear tethers only. The maximum cross-link density is then always expected at $N = 1$. However, if steric hindrance does not limit the cure reaction, bifurcated tethers form preferentially and thus the highest rubbery moduli occur at $N = 0.5$. For DGEBA/OAPS (PAPS) composites, linear tether formation is favored despite the absence of bulky groups directly adjacent to the epoxides or amines. This is probably because the aniline NH_2 groups are sufficiently congested sterically that a second epoxy moietycannot approach the reaction site. Alternately, the microscopic viscosity is so high that diffusion rates are very low. Thus, only linear tethers form. Increased viscosity on curing will also limit tether motion and thus cross-linking reactions.

Finally, the absence of T_gs at $N \approx 1$ suggests very rigid tethers. The tan δ profiles in Figure 3 more clearly show the disappearance of T_gs. In comparison (Table **3**), T_g disappears only at $N = 0.5$ for OG/DDM, where main chain relaxations are limited by the extremely high cross-link densities (4.4×10^{-3} mol/cm^3 vs $\sim 3 \times 10^{-3}$ mol/cm^3 for DGEBA/OAPS and OC/DDM, or 2×10^{-3} mol/cm^3 for DGEBA/DDM) arising from formation of bifurcated tethers. For octa(dimethylsiloxyethylcyclohexylepoxide) cube (OC)/DDM nanocomposites, which have their highest cross-link densities (2.8×10^{-3} mol/cm^3) at $N = 1.0$ with only linear tethers, T_gs are observed for all formulations suggesting that OC/DDM tethers are relatively flexible and can relax if provided with enough thermal energy.

In contrast, DGEBA/OAPS (PAPS) exhibits no T_g at $N = 1.0$ despite having cross-link densities (3.0×10^{-3} mol/cm^3) that are lower than those of OG/DDM at $N = 0.5$ and similar to those of OC/DDM at $N = 1.0$ (2.8×10^{-3} mol/cm^3) with only linear tethers. Thus, the lack of a T_g suggests that DGEBA/OAPS (PAPS) tethers are very rigid and their segmental relaxation is severely limited by the extra aromatic segments even at low cross-link densities. These results demonstrate that tether relaxation motions and thus global glass transition behavior can be easily controlled by varying the tether structure.

At this point, it is important to note that although curing appears to be relatively complete based on the ceramic yield data and FTIR studies, some defects resulting from incomplete curing must exist. However, their influence on mechanical properties and thermal stability seems minimal at best given that the 5% mass loss temperatures are higher than the analogous DDM materials (Table 5).

In summary, the DMA results provide several structure−property relationships for OAPS (PAPS) cube nanocomposites. First, slight defects in the cube core such as SiOH groups do not affect the macroscopic behavior, and nanocomposites prepared from OAPS and PAPS perform essentially at the same level suggesting that PAPS can serve as an alternative to OAPS. Second, aromatic segments reduce tether relaxation motions vs aliphatic ones and consequently glass transition behavior is suppressed. Although it is well-known that aromatic structures are more rigid than aliphatic ones, complete elimination of T_gs is unique to cube nanocomposites. This is because individual tether segmental motions dominate the network glass transition behavior due to limited cooperative motions, and thus slight changes (two more aromatic rings in this case) in the tether structure have immediate and significant effects on global properties. These results further suggest that comparative studies of well-defined cube nanocomposites offer a rare view of individual tether segmental motions that cannot be observed in organic thermosets, as discussed below. Last, linear tethers preferably form due to steric hindrance in the curing reaction. Thus, the effects of network architecture and cross-link densities on global properties are minimal and only tether properties induce different macroscopic behavior, offering ideal systems for comparative tether structure studies.

Comparative Studies of Tether Structure and Length. Because nanocomposite networks with a wide variety of structures can be prepared, standard network structures must be developed to study the effects of tether structure and length properly. In other words, nanocomposites of interest must have similar cross-link densities and tethers, similar architectures. Practically, $N = 1.0$ formulations can provide network structures that can best accommodate both conditions. First, only linear tethers are expected to form in DGEBA/OAPS (PAPS) and OG/OAPS. In OG/DDM, linear tethers are also dominant at $N = 1.0$ vs bifurcated tethers at $N = 0.5$.[18] Second, networks with linear tethers provide similar cross-link densities.

Thermal Gravimetric Analyses (TGA). Comparison of OG/DDM with OAPS/DGEBA provides a direct

Table 5. TGA of Nanocomposites (N_2/5° C/min) Prepared from OAPS/PAPS and OG

	OG/OAPS					OG/PAPS			
N	T_d(5%) (°C)[a]	T_d(20%) (°C)[b]	char yield (%)[c]	CY (%)[d]	[e]CY(theory) (%)	T_d(5%) (°C)[a]	T_d(20%) (°C)[b]	char yield (%)[c]	CY (%)[e]
0.30	373	427	52	47.9	49.0	369	424	52	47.7
0.50	380	434	56	47.2	48.1	382	435	56	47.2
0.75	387	444	60	46.7	47.4	385	439	56	46.5
1.00	385	448	61	46.2	46.9	378	438	56	46.2

[a] T_d(5): 5% mass loss temperature under N_2 (°C). [b] T_d(20): 20% mass loss temperature under N_2 (°C). [c] Char yield at 1000 °C under N_2 (%). [d] CY: ceramic yield at 1000 °C under air (%). [e] CY(theory): theoretical ceramic yield based on silica contents.

measure of the effects of tether architectural changes on nanocomposite thermal properties when slightly different tethers form via the same cure chemistry (Scheme 5). The TGA results for OG/DDM and DGEBA/OAPS are shown in Tables 3 and 4, respectively.

Comparison of these results shows that theoretical ceramic yields based on silica contents are significantly different for two nanocomposites despite the similar tether shapes and cross-link densities. This is because OG has eight spacer (Me_2SiO) groups containing Si−O segments producing ceramic yields twice those of OAPS. However, despite differences in silica contents, 5% and 20% mass loss temperatures are similar indicating high thermal stabilities for the aromatic tether structures. In contrast, char yields under N_2 are higher for OAPS/DGEBA than OG/DDM as expected given that aromatic structures normally offer high char yields.[42−48] These results suggest that thermal stabilities in cube nanocomposites are determined primarily by the nature of tethers and can be effectively improved by incorporating aromatic structures in tethers. The effects of silica in the form of cubes are discussed below.

In comparison, the literature reports increases in char yields, but often decreases in initial mass loss temperatures when epoxy resins are reinforced with sol−gel derived silica.[49−52] For example, char yields for DGEBA/DDM (N_2, TGA)[52] increase from 13% to 37% with 10 wt % silica loading (∼30 nm particle sizes), but 10% mass loss temperatures decrease from ∼370 to ∼300 °C probably because of incomplete condensation within the silica particles.

The effects of cubes on thermal stabilities can be observed separately by comparing DGEBA/OAPS and DGEBA/DDM (Table 3). Their networks consist primarily of DGEBA/aniline segments, but cubes act as additional cross-linkers in DGEBA/OAPS. Thus, any difference in thermal stabilities can be attributed to the effects of the cubes. As expected, no ceramic yield is obtained in air for DGEBA/DDM. However, 17% char yields are still obtained in N_2. The DGEBA/OAPS ceramic and char yields are 17.6 and 43.0% respectively. In comparison, 5% and 20% mass loss temperatures for DGEBA/OAPS are higher by 20 and 40 °C, respectively than DGEBA/DDM.

These results suggest that cubes effectively improve network thermal stabilities. The increase in char yields from 17 to 43% is more than expected based on silica content (∼18%). Given that organic tethers determine macroscopic thermal stabilities and DGEBA/aniline segments are expected to decompose at similar temperatures, increases in decomposition temperatures must be the result of cube incorporation.

Tether length effects on thermal stabilities were also studied using OG/OAPS and OG/DDM at $N = 1.0$ (see Schemes 5 and 6). Although direct comparison of OG/OAPS and OG/DDM should be limited to $N = 1.0$ due to the tether shape and cross-link density effects, several formulations were compared. Likewise, OG/PAPS nanocomposites were also prepared. TGA results for these composites are summarized in Table 5. As expected from above, both nanocomposites produce char yields greater than the theoretical ceramic yields. Also, these char yields increase as OAPS loading increases, despite the fact that the silica content (and ceramic yields) decrease correspondingly because OG contains twice as much silica as OAPS. Both nanocomposites exhibit very similar thermal behavior. That is, 5% and 20% mass loss temperatures and char yields at 1000 °C are nearly identical, again suggesting that the effects of Si−OH groups in PAPS are minimized at high cube loadings.

Comparison of OG/OAPS thermal stabilities with those of OG/DDM (Table 3) shows that OG/OAPS nanocomposites are more stable than OG/DDM for all temperature ranges. Because the OG/OAPS tether is nearly identical to half that of OG/DDM, tether structure effects are negligible in this case. Notable differences between them are that OG/OAPS has higher silica contents (46 vs 32%), cross-link densities (5.2×10^{-3} vs 3.0×10^{-3} mol/cm^3) and shorter tether lengths (1:2). As discussed above, higher silica contents and cross-link densities partly account for improved thermal stabilities. When tether lengths are shorter, cubes are more closely packed and pores in the networks are expected to be smaller. Accordingly, mass losses from segmental decomposition via diffusion of gaseous fragments are likely reduced by closely packed cubes. In comparison, limited diffusion paths are also identified as the source for thermal stability improvements for polymer−clay nanocomposites.[16,52−54] Thus, the improved thermal stability of OAPS/OG vs OG/DDM is likely a result of the combined effects of higher silica contents[49−52] and cross-link densities, increased aromatic content, and retarded diffusion of gaseous fragments produced during decomposition.

Dynamic Mechanical Analysis (DMA). DMA results for OG/DDM and DGEBA/OAPS are shown in Table 3 and Figure 2, respectively. Note that the DGEBA/OAPS tether architecture differs from that of OG/DDM primarily by two aromatic rings.

When $N = 1$, only OG/DDM exhibits a T_g and, consequently, moduli at temperatures of 200 °C are significantly higher for DGEBA/OAPS (1 GPa vs 0.06 GPa). As discussed above, the glass transition behavior of cube nanocomposites is dominated by individual tether relaxation behavior and the effects of multiple tether cooperative motions are likely minimal. Thus, the absence of T_g for DGEBA/OAPS suggests that DGEBA/OAPS tethers are relatively rigid and do not relax at elevated temperatures while OG/DDM tethers are quite flexible.

In comparison, OG/DDM relaxation disappears at $N = 0.5$ where bifurcated tether structures add extra

cross-links on tethers (Scheme 6), reducing the average segment sizes between cross-links by one-fifth (MW 191). In this case, the relaxation motions of smaller segments are strongly inhibited by short lengths and extra cross-links. These results suggest that tether segmental motions are important in determining the global glass transition behavior and their relaxations are reduced by aromatic structures, short lengths and high cross-link densities.

The effects of cube cross-linkers on network formation and the macroscale thermomechanical stabilities vs organic epoxy can be better understood by comparing glass transition behavior and cross-link densities of DGEBA/DDM (Table 3) with those of DGEBA/OAPS (PAPS) (Figure 2 and Table 5). DMA results show that only DGEBA/DDM exhibits a glass transition at $N = 1$. However, conventional cross-linking properties, M_c and ν are similar despite largely different macroscopic relaxations suggesting that they fail to explain cube nanocomposite behavior. Thus, for cube nanocomposites, high cross-link densities localized at cubes and limited tether cooperative motions must be considered in any efforts to predict or model global properties.

First, cubes offer eight cross-link points in a small volume whereas cross-link junctions in organic epoxy resins are usually uniformly dispersed and connect only three segments. The number of DGEBA/OAPS (PAPS) cross-link junctions (3.02×10^{-3} mol/cm^3) is higher than that for DGEBA/DDM (2.12×10^{-3} mol/cm^3). Next, rigid DGEBA/OAPS (PAPS) tethers exhibit limited ability to relax and their cooperative motions are also likely limited leading to practically no macroscopic glass transitions. In comparison, for organic epoxies, cooperative relaxation motions of various segments are suggested as primary source for glass transition behavior.[31] As a result, DGEBA/OAPS (PAPS) nanocomposites do not exhibit relaxation behavior, while DGEBA/DDM has a clear T_g.

When OG/OAPS (PAPS) nanocomposites were characterized by DMA to probe the effects of short and rigid tethers (Scheme 7 and Table 5), they were found to be extremely brittle and frequently did not survive introduction of the samples to the DMA, resulting in unreliable measurements. These results suggest that extremely short and rigid tethers stiffen the network to the point where network relaxation is almost impossible and no energy is dissipated by tether segmental motions. Given that organic epoxy resins filled with silica powders exhibit improved fracture toughness at silica contents >60 wt %,[55,56] cube loadings (~50 wt %) do not seem to be critical in stiffening the network. Therefore, it appears that OG/OAPS (PAPS) network structures represent a practical limit in reducing tether segmental motions to obtain network stabilities at elevated temperatures.

Conclusions

This study provides several nanostructure−property relationships for cube nanocomposites. First, OAPS and PAPS exhibit similar reactivities and are processed in a similar manner. Slight structural defects in PAPS cube cores barely degrade thermomechanical properties. Thus, OAPS/PAPS nanocomposites are expected to perform at the same level. Therefore, PAPS can serve as a low cost alternative to OAPS.

Second, cubes limit the cooperative motions of multiple tethers, and thus, individual tether segmental motions dominate the global glass transition behavior. Tether relaxation motions can be controlled by tether structure, length and the cross-link density. It also seems that there is a limiting point in tether design where further decreases in tether lengths and increases in aromatic character result in nanocomposites too brittle to offer useful mechanical properties even for characterization. Third, increasing tether aromatic character greatly improves nanocomposite thermomechanical stabilities. Increasing silica contents also improves macroscopic thermal stabilities. Last, control of chemistry and stoichiometry provide the opportunity to develop nanocomposites with completely linear tethers. That is, nanotailoring of nanocomposite properties seems to be not only possible but relatively easy to accomplish.

Finally, although bulk ceramic materials are very brittle; very thin ceramic fibers and films exhibit excellent mechanical properties because the energy required to initiate cracks leading to catastrophic failure is often beyond normal use conditions. Consequently, it is reasonable to suggest that thin films and fibers of the materials produced here may also exhibit excellent mechanical properties that rival some ceramics. Furthermore, because these materials can be fabricated using modest processing conditions, their utility may surpass some ceramic materials.

Acknowledgment. The authors thank the FAA (Grant No. 95-G-026), AFOSR, Matsushita Electric, Inc., and Guardian Industries for support of the work reported here. We would also like to thank one of the reviewers for extensive comments that helped make this a better manuscript.

References and Notes

(1) Sanchez, C.; Lebeau, B. *MRS Bull.* **2000**, *26*, 377.
(2) Seraji, S.; Wu, Y.; Forbes, M.; Limmer, S. J.; Chou, T.; Cao, G. *Adv. Mater.* **2000**, *12*, 1695.
(3) Rajeshwar, K.; de Tacconi, N. R.; Chenthamarakshan, C. R. *Chem. Mater.* **2001**, *13*, 2765.
(4) Scott, B. J.; Wirnsberger, G.; Stucky, G. D. *Chem. Mater.* **2001**, *13*, 3140.
(5) Kojima, Y.; Usuki, A.; Kawasumi, M. *J. Mater. Res.* **1993**, *8*, 1185.
(6) Corriu, R. *J. Polyhedron* **1998**, *17*, 925.
(7) Sanchez, C.; Soler-Illia, G. J. de A. A.; Ribot, F.; Lalot, T.; Mayer, C. R.; Cabuil, V. *Chem. Mater.* **2001**, *13*, 3061.
(8) Vaia, R. A.; Giannelis, E. P. *Chem. Mater.* **2001**, *13*, 3306.
(9) Matthews, F. L.; Rawlings, R. D. *Composites materials: Engineering and science*; Chapman & Hall: London, U.K., 1994; p 14.
(10) Jackson, G. V.; Orton, M. L. In *Particulate-filled polymer composites*; Rothon, R., Ed.; Longman Scientific & Technical: Essex, U.K., 1995; p 317.
(11) Demjen, Z.; Pukanszky, B.; Nagy, J. *Composites Part A* **1998**, *29*, 323.
(12) Chiu, H.; Wang, J. *J. Appl. Polym. Sci.* **1998**, *68*, 1387.
(13) Delong, J.; Hook, K. J.; Rich, M. J.; Drzal, L. T. In *Composite Materials*; Ishida, H., Ed.; Elsevier Press: New York, 1990; p 87.
(14) LeBaron, P. C.; Wang, Z.; Pinnavaia, T. J. *Appl. Clay Sci.* **1999**, *15*, 11.
(15) Carrado, K. *Appl. Clay Sci.* **2000**, *17*, 1.
(16) Alexangdre, M.; Dubois, P. *Mater. Sci. Eng.* **2000**, *28*, 1.
(17) Laine, R. M.; Choi, J.; Lee, I. *Adv. Mater.* **2001**, *13*, 800.
(18) Choi, J.; Harcup, J.; Yee, A. F.; Zhu, Q.; Laine, R. M. *J. Am. Chem. Soc.* **2001** *123*, 11420.
(19) Zhang, C.; Babonneau, F.; Bonhomme, C.; Laine, R. M.; Soles, C. L.; Hristov, H. A.; Yee, A. F. *J. Am. Chem. Soc.* **1998**, *120*, 8380.
(20) Zhang, C.; Laine, R. M. *J. Am. Chem. Soc.* **2000**, *122*, 6979.
(21) Sellinger, A.; Laine, R. M. *Macromolecules* **1996**, *29*, 2327.
(22) Zhang, C.; Laine, R. M. *J. Organomet. Chem.* **1996**, *521*, 199.

(23) Sellinger, A.; Laine, R. M. *Chem. Mater.* **1996**, *9*, 1592.
(24) Laine, R. M.; Zhang, C.; Sellinger, A.; Viculis, L. *Appl. Organomet. Chem.* **1998**, *12*, 715.
(25) Tamaki, R.; Tanaka, Y.; Asuncion, M. Z.; Choi, J.; Laine, R. M. *J. Am. Chem. Soc.* **2001**, *123*, 12416.
(26) Li, G. Z.; Wang, L.; Toghiani, H.; Daulton, T. L.; Koyama, K.; Pittman, C. U., Jr. *Macromolecules* **2001**, *34*, 8686.
(27) Kim, G.-M.; Qin, H.; Fang, X.; Mather, P. T. *J. Polym. Sci. B: Polym. Phys. Ed.* **2003**, *41*, 3299.
(28) Laine, R. M.; Tamaki, R.; Choi, J. Well-defined nanosized building blocks for organic/inorganic nanocomposites. WO 02/100867 A1.
(29) Tanaka, Y. In *Epoxy resins, chemistry and technology*; May, C. A., Ed.; Marcel Dekker: New York, 1988; p 9.
(30) Goodman, S. H. In *Handbook of thermoset plastics*; Goodman, S. H., Ed.; Noyes Publ.: Westwood, NJ, 1998; p 193.
(31) Smith, G.; May, C. A. In *Epoxy resins*; Gould, R. F., Ed.; ACS Publications: Washington, DC, 1970; p 140.
(32) Kaelble, D. H. In *Epoxy resins, chemistry and technology*; May, C. A., Ed.; Marcel Dekker: New York, 1988; p 603.
(33) Richard, E. G. *An introduction to physical properties of large molecules in solution*; Cambridge University Press: London, U.K., 1980; p 115.
(34) Strobl, G. *The physics of polymers: concepts for understanding their structures and behaviors*; Springer: Berlin, Germany, 1996; p 297.
(35) Shan, L.; Verghese, K. N. E.; Robertson, C. G.; Reifsnider, K. L. *J. Polym. Sci., Part B: Polym. Phys.* **1999**, *37*, 2815.
(36) Brown, J. F., Jr. *J. Am. Chem. Soc.* **1965**, *87*, 4317.
(37) Prado, L. A. S. De A.; Radovanovic, E.; Pastore, H. O.; Yoshida, I. V. P.; Torriani, I. L. *J. Polym. Sci., Part A: Polym. Chem.* **2000**, *38*, 1580.
(38) Zhu, B.; Katsoulis, D. E.; Keryk, J. R.; McGarry, F. J. *Polymer* **2000**, *41*, 7559.
(39) Lee, E.-C.; Kimura, Y. *Polym. J.* **1998**, *30*, 730.
(40) Silverstein, R. M.; Webster, F. X. *Spectrometric identification of organic compounds*; John Wiley & Sons: New York, 1996; p 71.
(41) Choi, J.; Lee, I.; Yee, A. F.; Laine, R. M. *Macromolecules* **2003**, *15*, 5666−82.
(42) Puglia, D.; Manfredi, L. B.; Vazquez, A.; Kenny, J. M. *Polym. Degrad. Stab.* **2001**, *73*, 521.
(43) Gupta, N.; Varma, I. K. *J. Appl. Polym. Sci.* **1998**, *68*, 1759.
(44) Levchik, S. V.; Camino, G.; Luda, M. P.; Costa, L.; Muller, G.; Costes, B.; Henry, Y. *Polym. Adv. Technol.* **1996**, *7*, 823.
(45) Mikroyannidis, J. A. *J. Appl. Polym. Sci.* **1990**, *41*, 2625.
(46) Liou, G.-S.; Hsiao, S.-H. *J. Polym. Sci., Part A: Polym. Chem.* **2002**, *40*, 459.
(47) Hemvichian, K.; Laobuthee, A.; Chirachanchai, S.; Ishida, H. *Polym. Degrad. Stab.* **2002**, *76*, 1.
(48) Ubale, V. P.; Sagar, A. D.; Maldar, N. N.; Birajdar, M. V. *J. Appl. Polym. Sci.* **2001**, *79*, 566.
(49) Shih, W.-C.; Ma, C.-C. M.; Yang, J. C.; Chen, H.-D. *J. Appl. Polym. Sci.* **1999**, *73*, 2739.
(50) Ochi, M.; Takahashi, R.; Terauchi, A. *Polymer* **2001**, *42*, 5151.
(51) Ochi, M.; Takahashi, R. *J. Polym. Sci., Part B: Polym. Phys.* **2001**, *39*, 1071.
(52) Hsiue, G. H.; Liu, Y. L.; Liao, H. H. *J. Polym. Sci., Part A: Polym. Chem.* **2001**, *39*, 986.
(53) PeBaron, P. C.; Wang, Z.; Pinnavaia, T. J. *Appl. Clay Sci.* **1999**, *15*, 11.
(54) Burnside, S. D.; Giannelis, E. P. *Chem. Mater.* **1995**, *7*, 1597.
(55) Koh, S.-W.; Kim, J.-K.; Mai, Y.-W. *Polymer* **1993**, *34*, 3446.
(56) Nakamura, Y.; Yamaguchi, M.; Okubo, M.; Matsumoto, T. *Polymer* **1992**, *33*, 3415.

MA030309D